Supplement of The Cryosphere, 18, 1207–1213, 2024
https://doi.org/10.5194/tc-18-1207-2024-supplement

The Cryosphere Open Access EGU

Supplement of

Brief communication: Significant biases in ERA5 output for the McMurdo Dry Valleys region, Antarctica

Ricardo Garza-Giró and Slawek M. Tulaczyk

Correspondence to: Ricardo Garza-Girón (rgarzagi@ucsc.edu, r.garza_giron@colostate.edu)

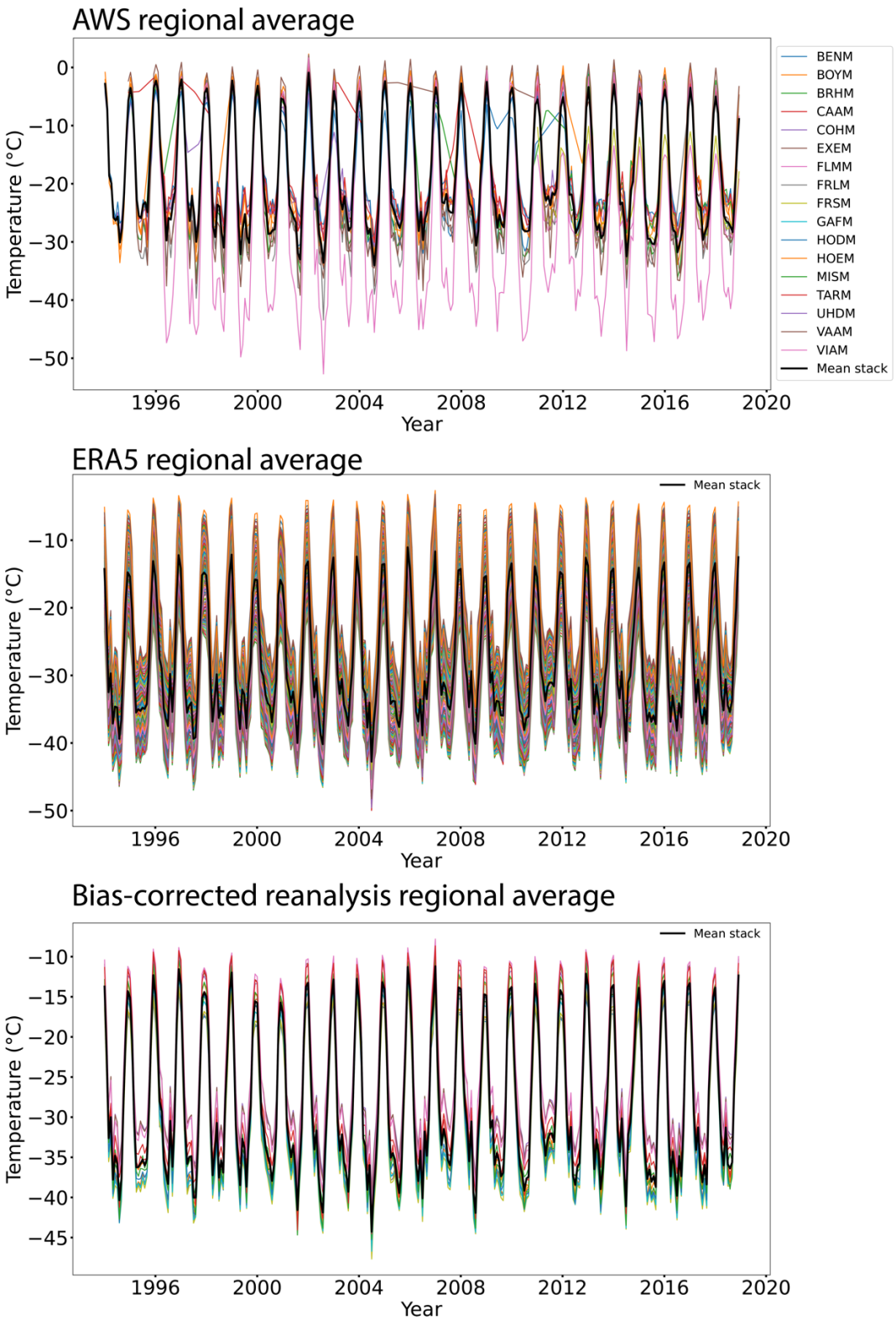

Figure S1. Time series of regional averages for all the AWS (top panel), all the ERA5 grid cells (middle panel) and all the BCR grid cells (bottom panel), that are within the main region of the McMurdo Dry Valleys (black box in Figure 1 of main text).

Spatial distribution of the elevation of the Automatic Weather Stations (AWS) and the temperature biases between the AWS and the values from the closest grid node of the ERA5 reanalysis and the Bias-Corrected reanalysis (BCR) datasets.

Figure S1 shows the elevation map of all the AWS used in this study. We also show the regional geographical distribution of the temperature biases between the Automatic Weather Stations (AWS) in the McMurdo Dry Valleys region, Antarctica, and the nearest node of the ERA5 (Figure S2) and the bias-corrected reanalysis (BCR, Figure S3) datasets after a dry adiabatic lapse rate correction was applied. Even though most of the ERA5 biases in the stations inside the valleys are neutral to warm, a dependance on station elevation is not apparent.

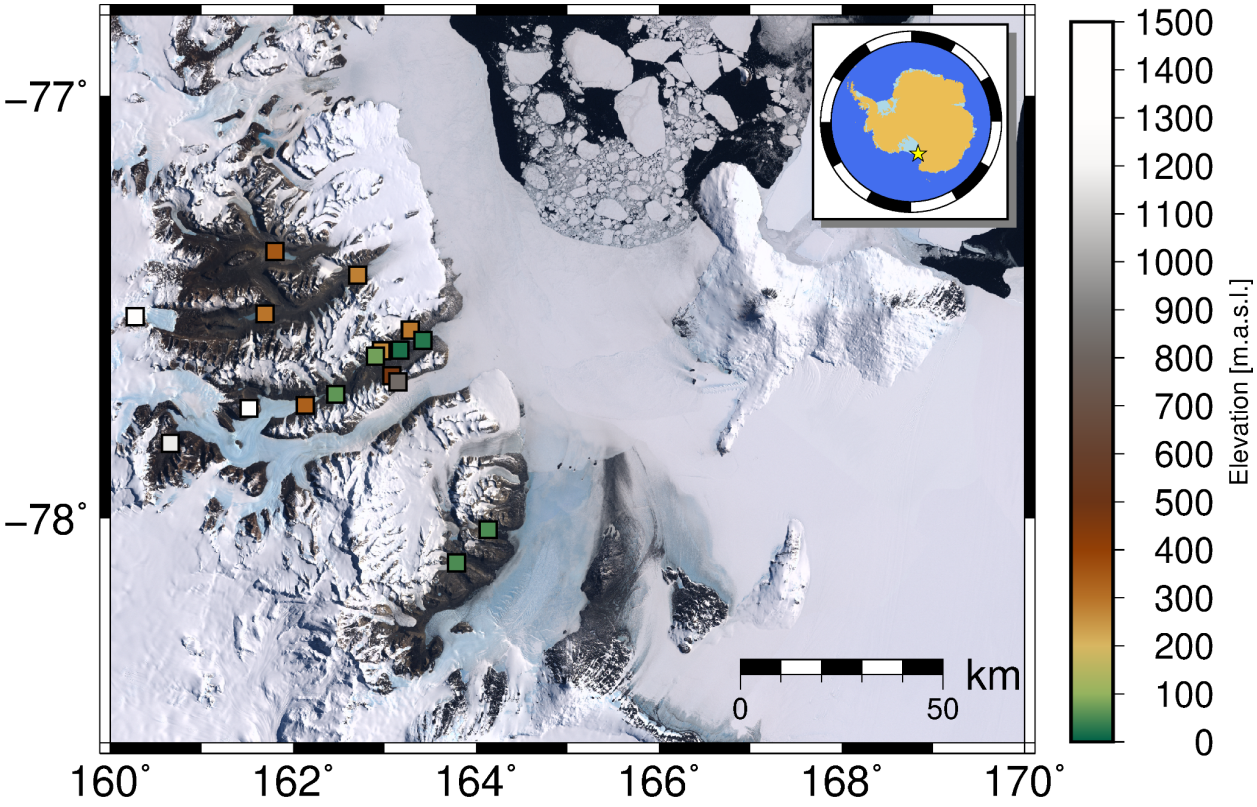

Figure S2. Elevation map for the 17 Automatic Weather Stations (AWS) used in this study.

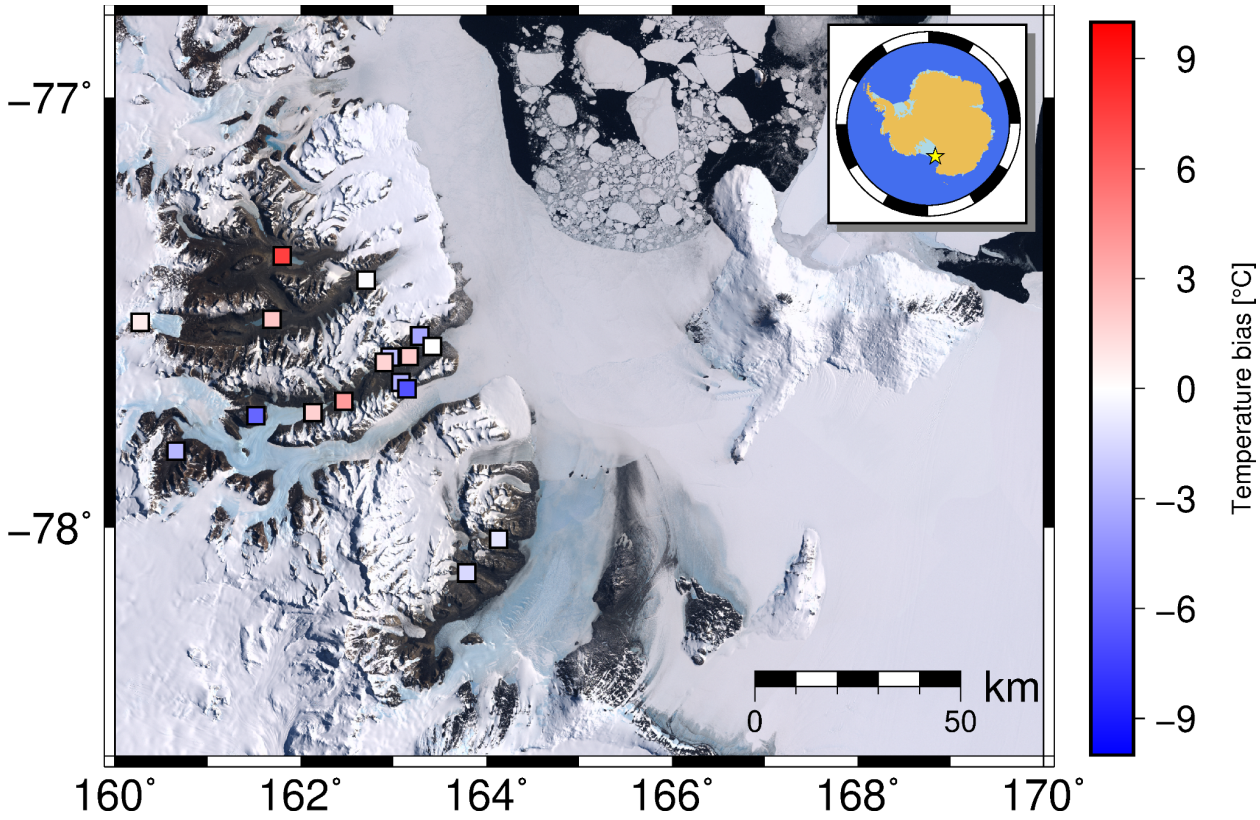

Figure S3. Temperature biases between the AWS and the ERA5 data after a dry adiabatic lapse rate correction was applied.

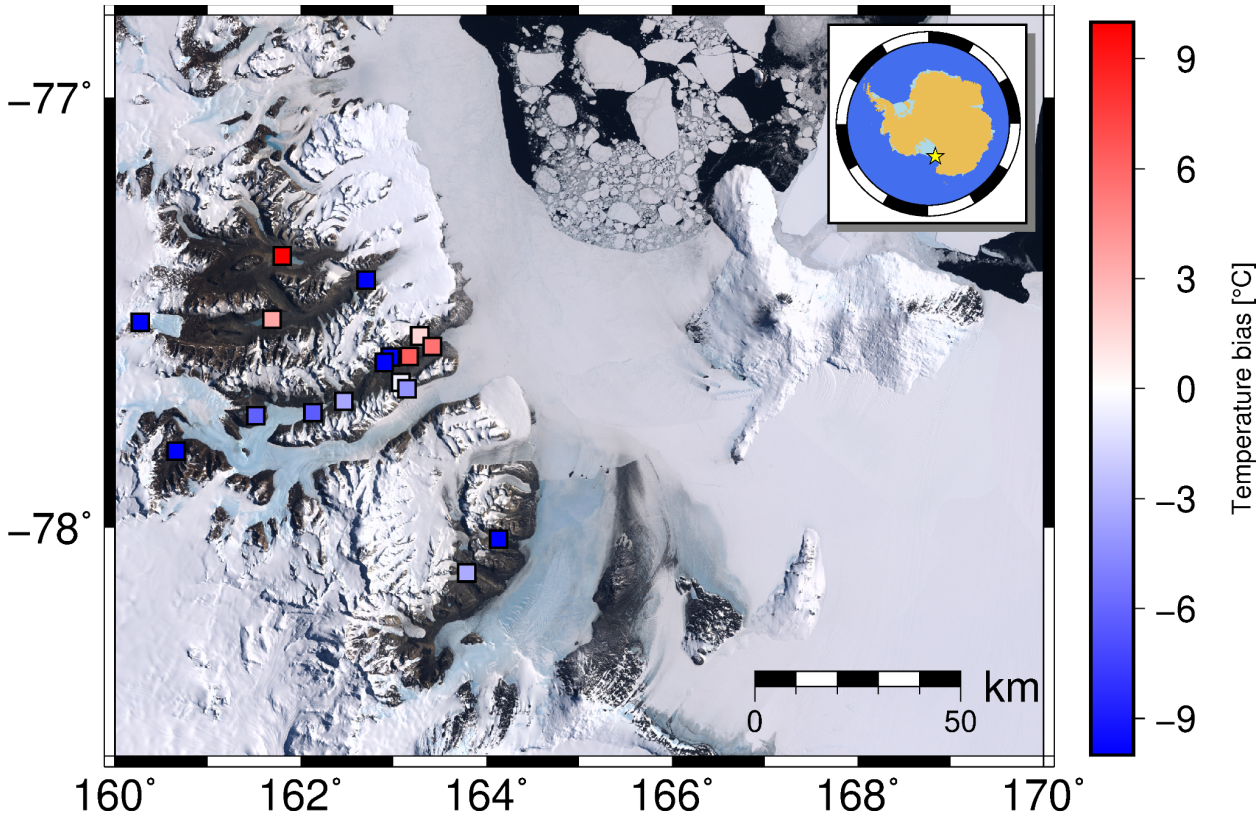

Figure S4. Temperature biases between the AWS and the BCR data after a dry adiabatic lapse rate correction was applied.

Comparison of the monthly averaged surface temperature time series recorded at the AWS and the values from the closest grid node of the ERA5 reanalysis and the BCR datasets.

In this section of the supporting information we show the multi-decadal time series of the 2-metre air temperature for the 17 AWS, and the temperatures calculated at the nearest grid cell for two climate reanalysis models, ERA5 and BCR. We also show the correlograms from which one can see the seasonal dependence on the bias as noted in the main text.

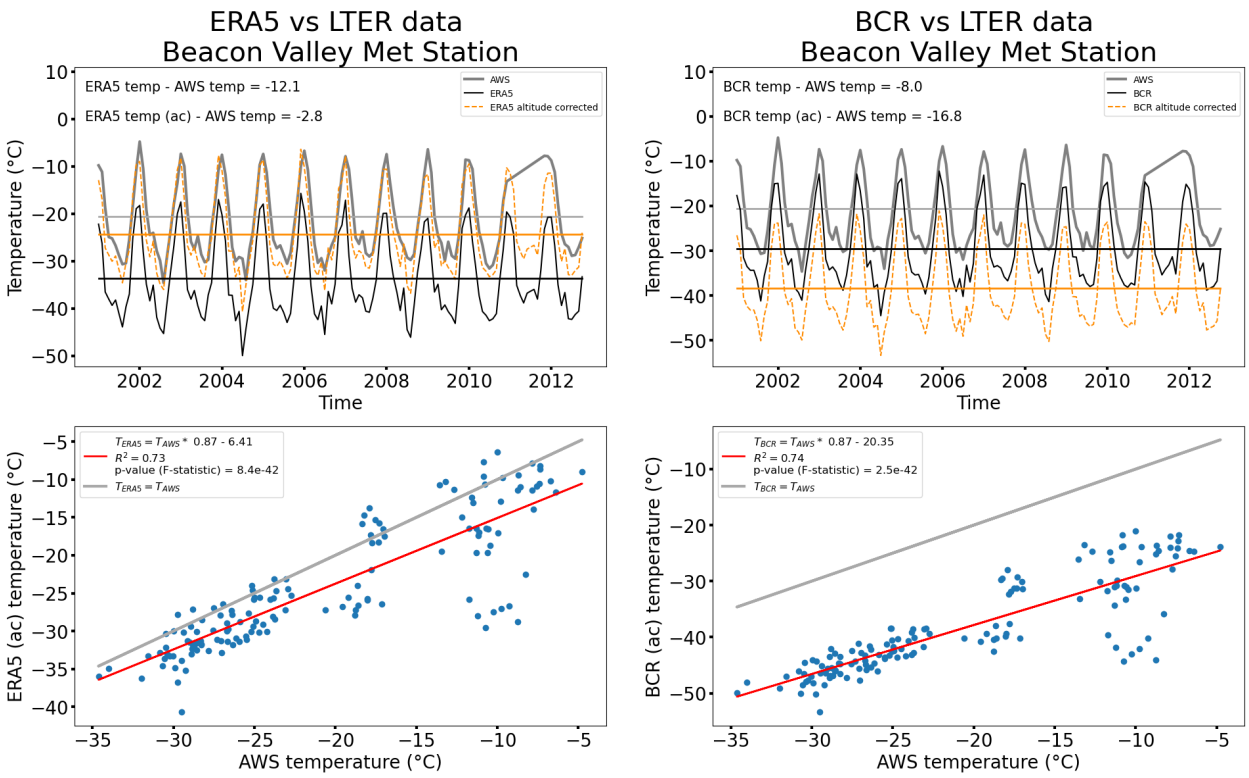

Figure S5. Comparison of the monthly averaged 2-metre air temperatures recorded at station Beacon Valley (BENM) and the values from the closest grid node of the ERA5 and BCR datasets. Time series of the AWS data (grey curve) compared to the reanalyses data (black curve) and the altitude-corrected (ac) reanalyses data (dashed orange curve) for the ERA5 (a) and BCR (b) datasets. The correlograms showing the best fit line to the relationship between the AWS temperatures and the ERA5 and BCR temperatures are shown in (c) and (d), respectively. Note the seasonal variation in the relationship, particularly the large bias during the summer months.

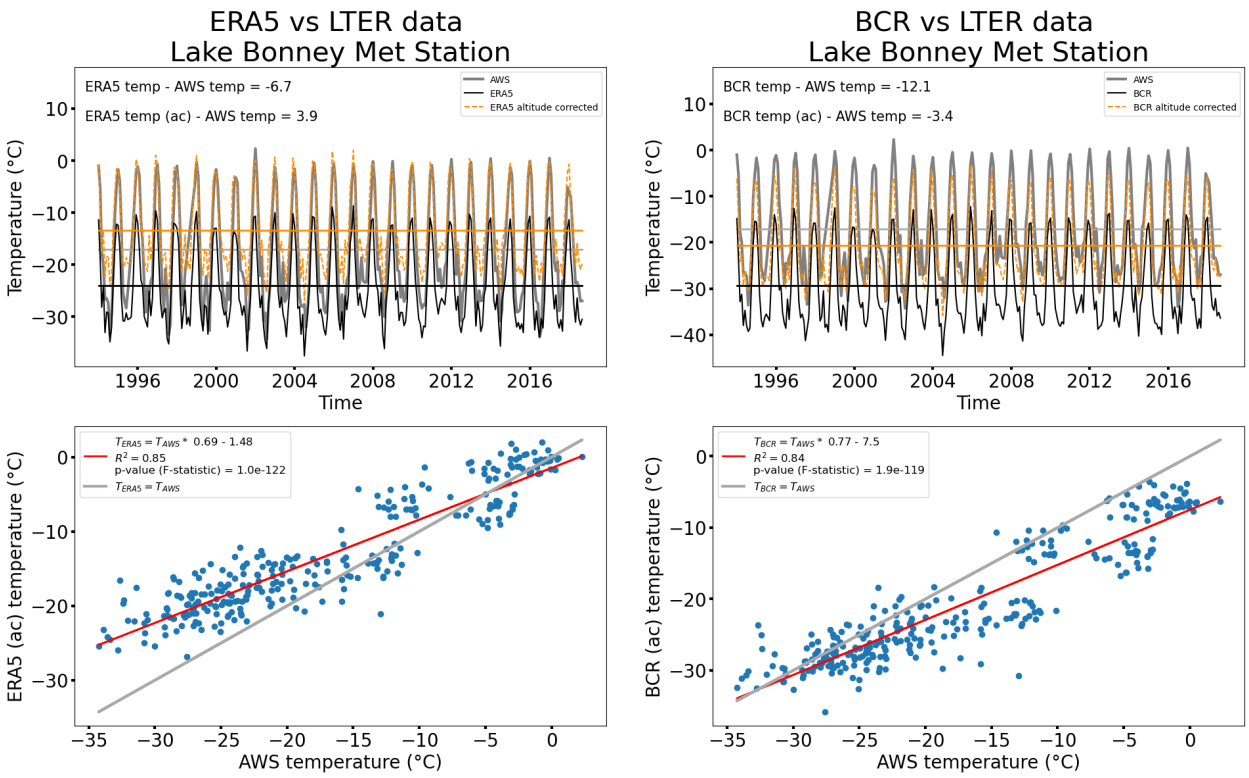

Figure S6. Comparison of the monthly averaged 2-metre air temperatures recorded at station Lake Bonney (BOYM) and the values from the closest grid node of the ERA5 and BCR datasets. Time series of the AWS data (grey curve) compared to the reanalyses data (black curve) and the altitude-corrected (ac) reanalyses data (dashed orange curve) for the ERA5 (a) and BCR (b) datasets. The correlograms showing the best fit line to the relationship between the AWS temperatures and the ERA5 and BCR temperatures are shown in (c) and (d), respectively. Note the seasonal variation in the relationship, particularly the large bias during the summer months.

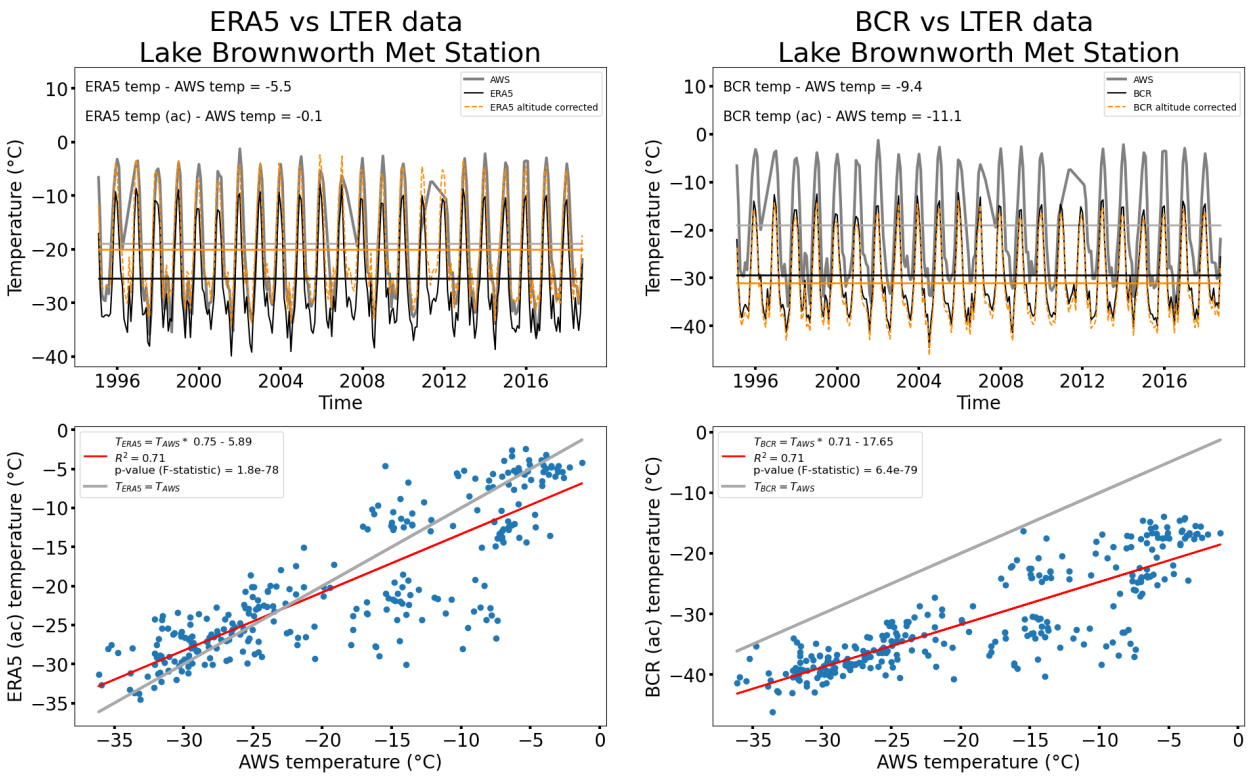

Figure S7. Comparison of the monthly averaged 2-metre air temperatures recorded at station Lake Brownworth (BRHM) and the values from the closest grid node of the ERA5 and BCR datasets. Time series of the AWS data (grey curve) compared to the reanalyses data (black curve) and the altitude-corrected (ac) reanalyses data (dashed orange curve) for the ERA5 (a) and BCR (b) datasets. The correlograms showing the best fit line to the relationship between the AWS temperatures and the ERA5 and BCR temperatures are shown in (c) and (d), respectively. Note the seasonal variation in the relationship, particularly the large bias during the summer months.

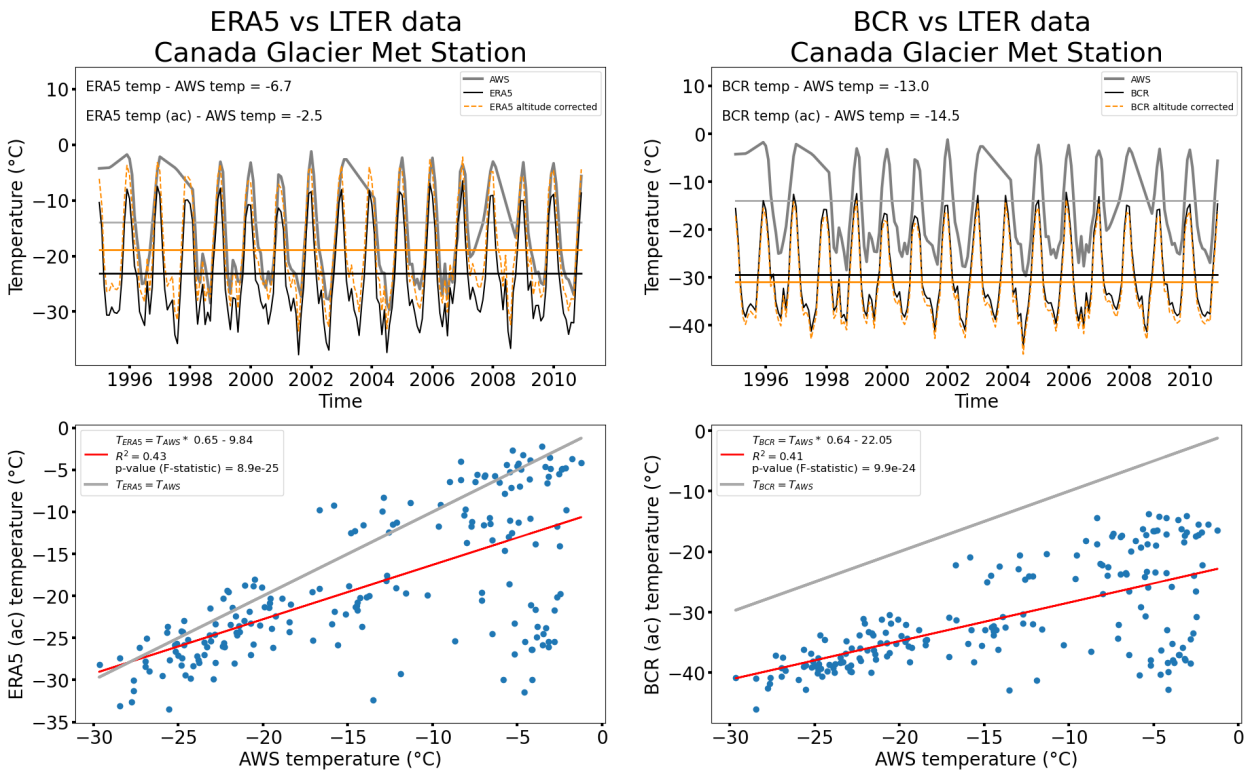

Figure S8. Comparison of the monthly averaged 2-metre air temperatures recorded at station Canada Glacier (CAAM) and the values from the closest grid node of the ERA5 and BCR datasets. Time series of the AWS data (grey curve) compared to the reanalyses data (black curve) and the altitude-corrected (ac) reanalyses data (dashed orange curve) for the ERA5 (a) and BCR (b) datasets. The correlograms showing the best fit line to the relationship between the AWS temperatures and the ERA5 and BCR temperatures are shown in (c) and (d), respectively. Note the seasonal variation in the relationship, particularly the large bias during the summer months.

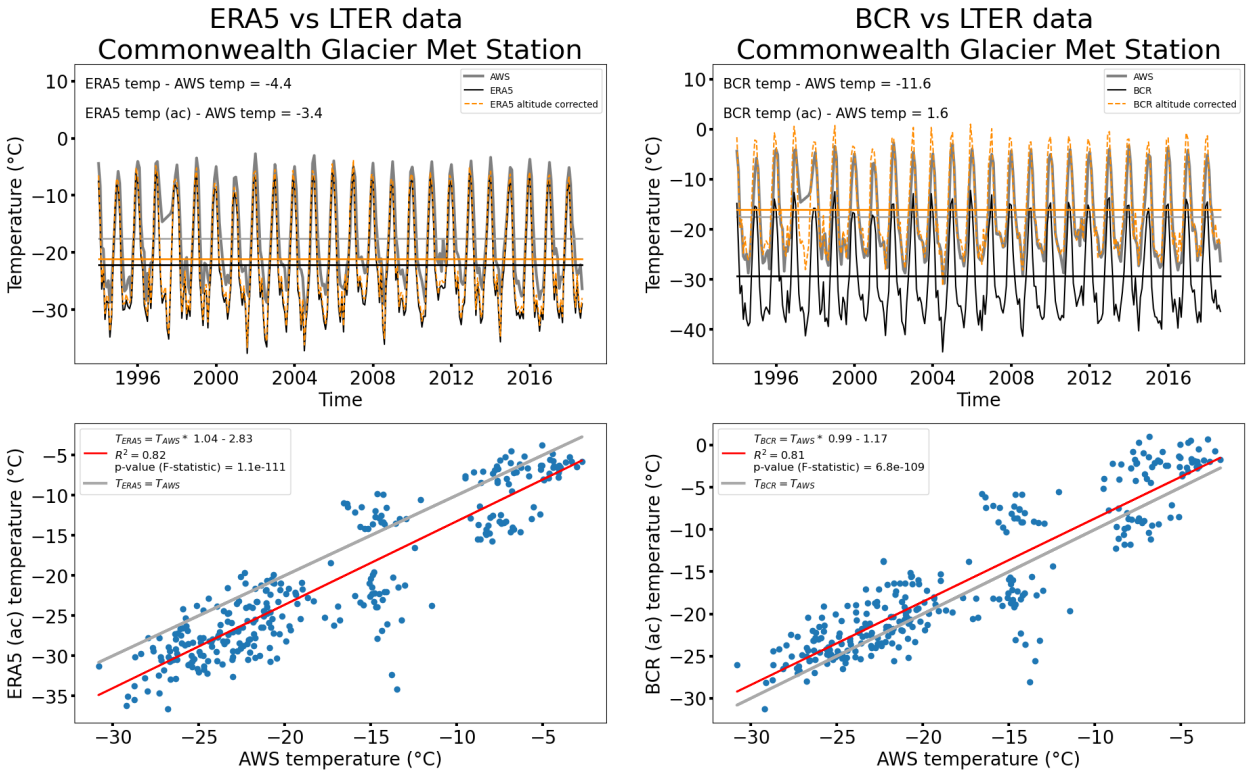

Figure S9. Comparison of the monthly averaged 2-metre air temperatures recorded at station Commonwealth Glacier (COHM) and the values from the closest grid node of the ERA5 and BCR datasets. Time series of the AWS data (grey curve) compared to the reanalyses data (black curve) and the altitude-corrected (ac) reanalyses data (dashed orange curve) for the ERA5 (a) and BCR (b) datasets. The correlograms showing the best fit line to the relationship between the AWS temperatures and the ERA5 and BCR temperatures are shown in (c) and (d), respectively. Note the seasonal variation in the relationship, particularly the large bias during the summer months.

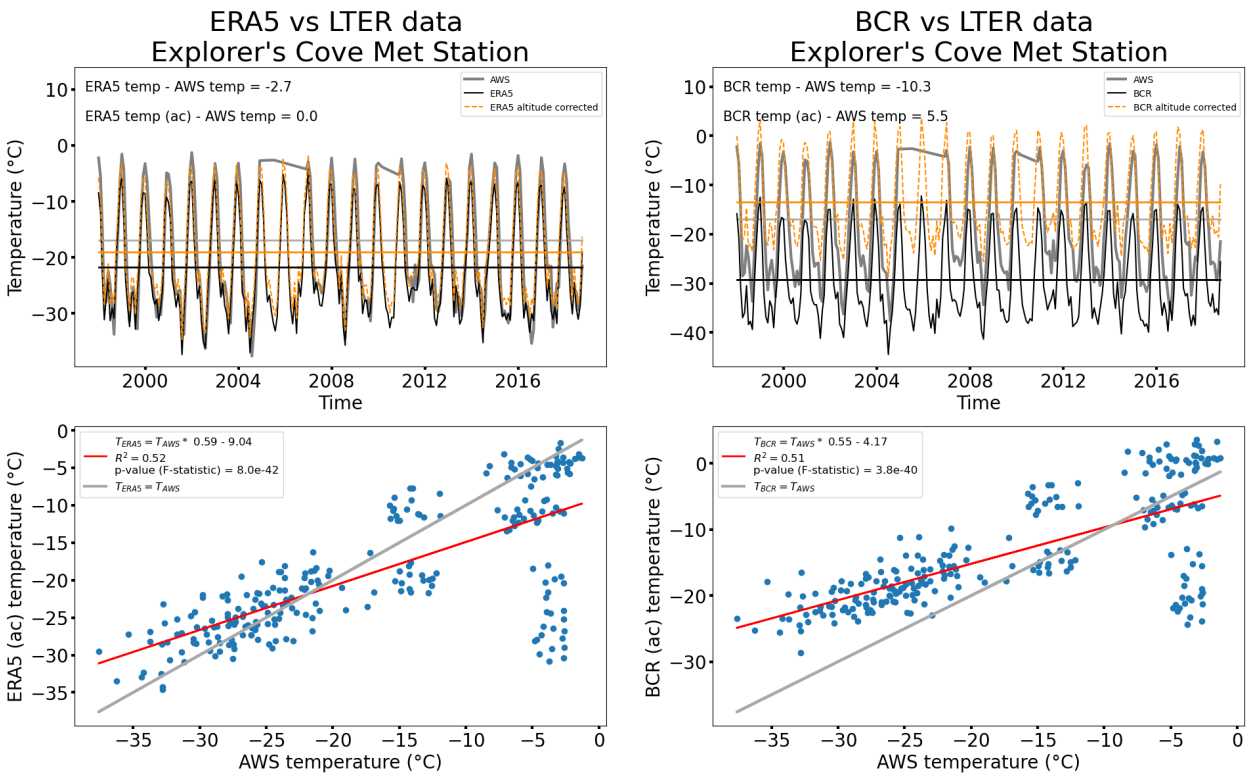

Figure S10. Comparison of the monthly averaged 2-metre air temperatures recorded at station Explorer's Cove (EXEM) and the values from the closest grid node of the ERA5 and BCR datasets. Time series of the AWS data (grey curve) compared to the reanalyses data (black curve) and the altitude-corrected (ac) reanalyses data (dashed orange curve) for the ERA5 (a) and BCR (b) datasets. The correlograms showing the best fit line to the relationship between the AWS temperatures and the ERA5 and BCR temperatures are shown in (c) and (d), respectively. Note the seasonal variation in the relationship, particularly the large bias during the summer months.

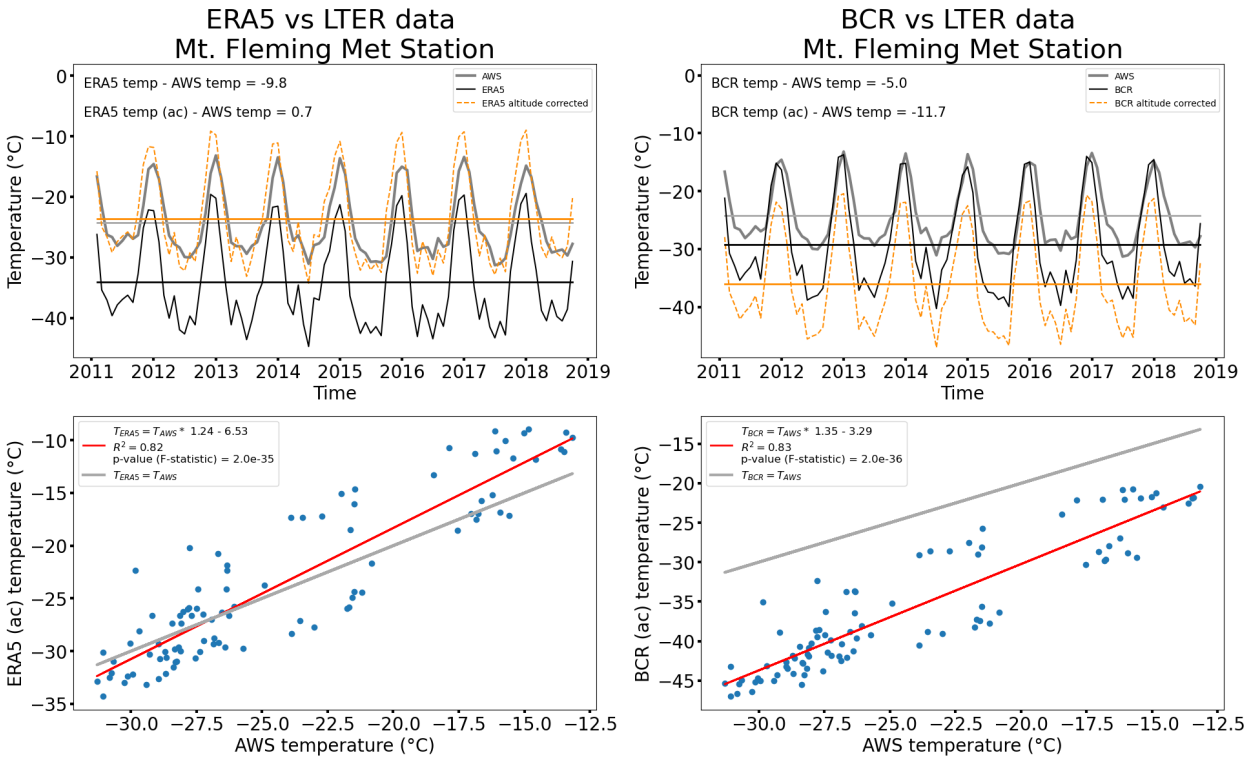

Figure S11. Comparison of the monthly averaged 2-metre air temperatures recorded at station Mount Flemming (FLMM) and the values from the closest grid node of the ERA5 and BCR datasets. Time series of the AWS data (grey curve) compared to the reanalyses data (black curve) and the altitude-corrected (ac) reanalyses data (dashed orange curve) for the ERA5 (a) and BCR (b) datasets. The correlograms showing the best fit line to the relationship between the AWS temperatures and the ERA5 and BCR temperatures are shown in (c) and (d), respectively. Note the seasonal variation in the relationship, particularly the large bias during the summer months.

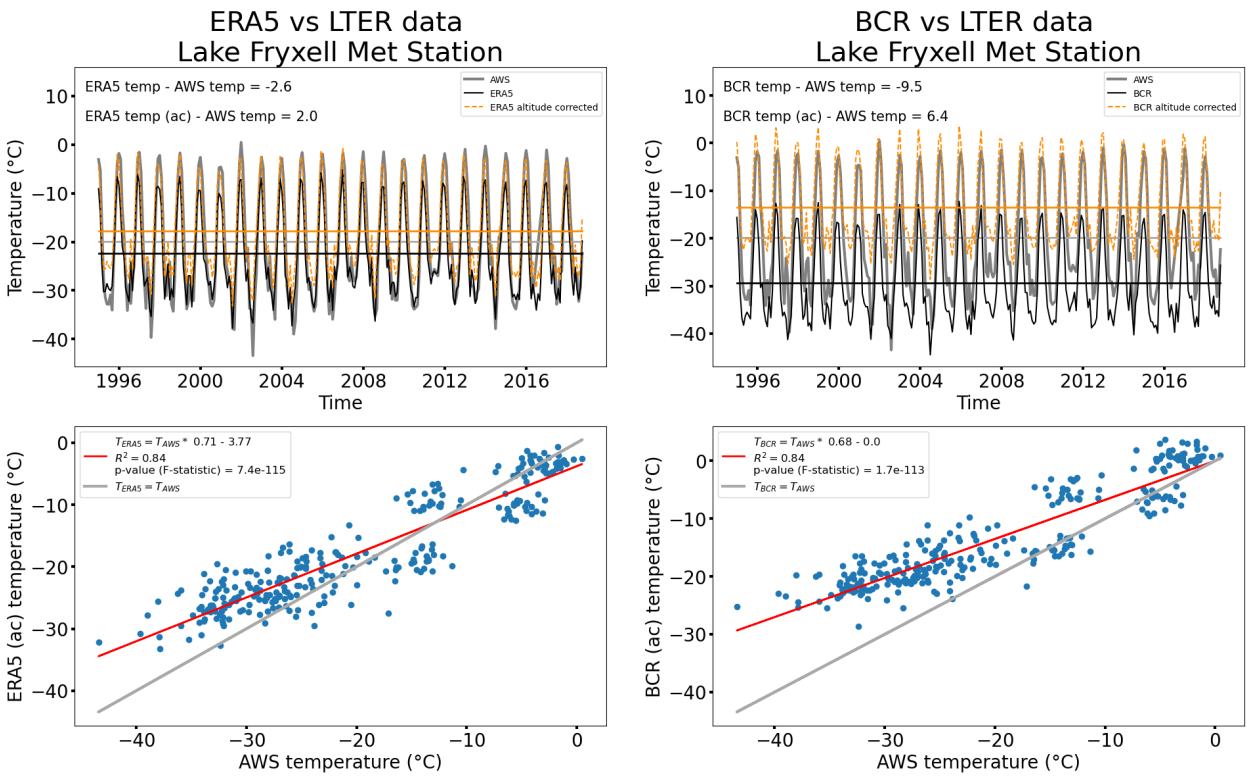

Figure S12. Comparison of the monthly averaged 2-metre air temperatures recorded at station Lake Fryxell (FRLM) and the values from the closest grid node of the ERA5 and BCR datasets. Time series of the AWS data (grey curve) compared to the reanalyses data (black curve) and the altitude-corrected (ac) reanalyses data (dashed orange curve) for the ERA5 (a) and BCR (b) datasets. The correlograms showing the best fit line to the relationship between the AWS temperatures and the ERA5 and BCR temperatures are shown in (c) and (d), respectively. Note the seasonal variation in the relationship, particularly the large bias during the summer months.

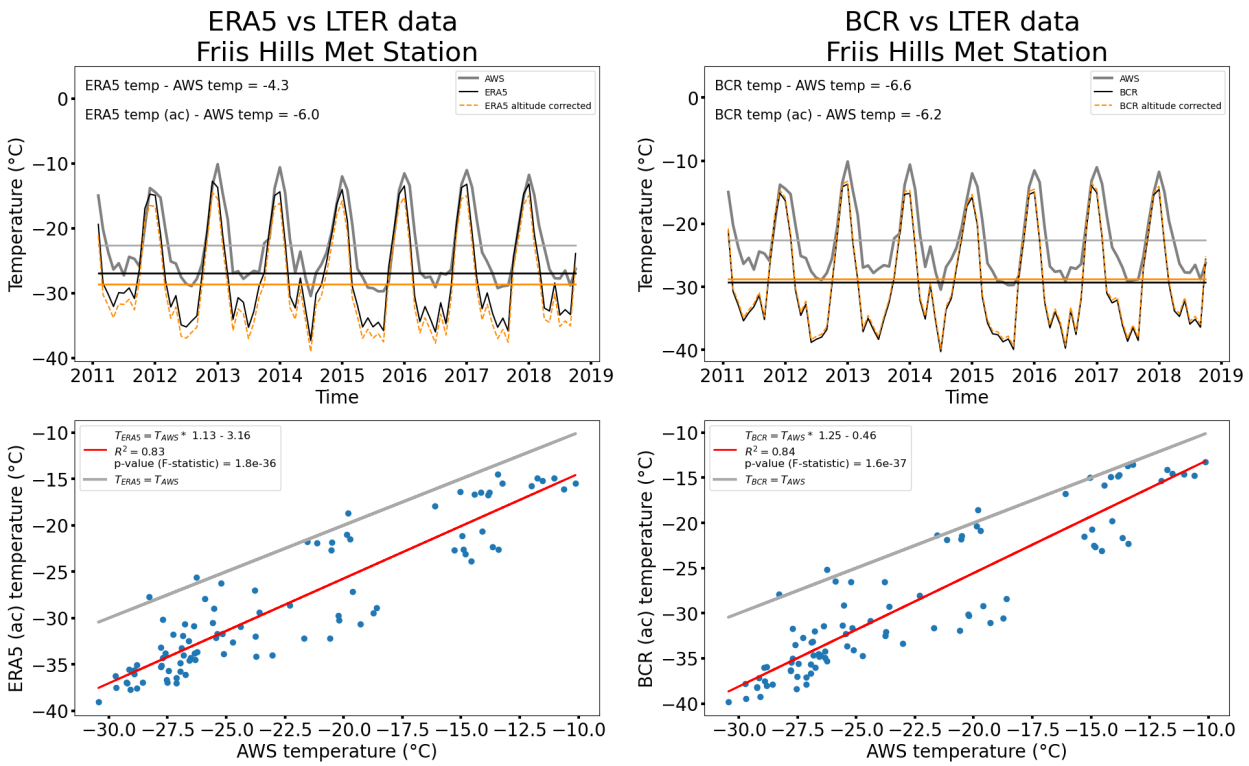

Figure S13. Comparison of the monthly averaged 2-metre air temperatures recorded at station Friis Hills (FRSM) and the values from the closest grid node of the ERA5 and BCR datasets. Time series of the AWS data (grey curve) compared to the reanalyses data (black curve) and the altitude-corrected (ac) reanalyses data (dashed orange curve) for the ERA5 (a) and BCR (b) datasets. The correlograms showing the best fit line to the relationship between the AWS temperatures and the ERA5 and BCR temperatures are shown in (c) and (d), respectively. Note the seasonal variation in the relationship, particularly the large bias during the summer months.

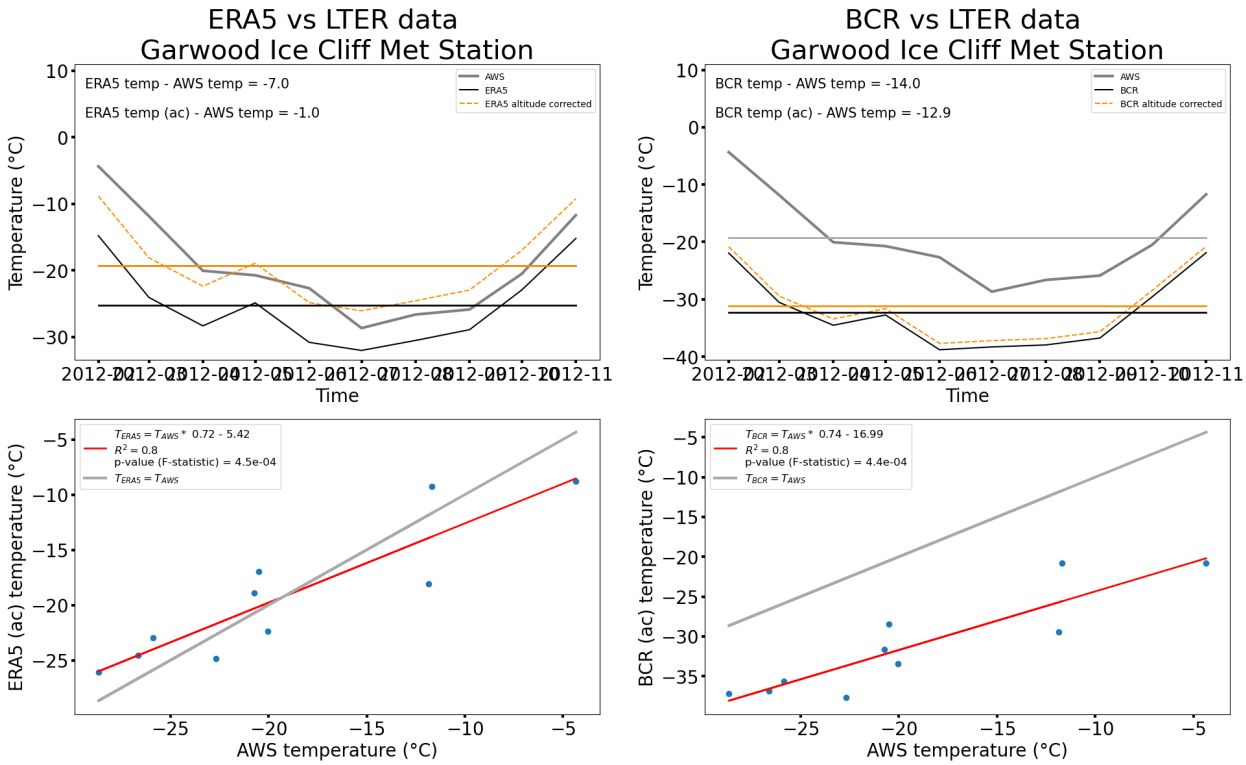

Figure S14. Comparison of the monthly averaged 2-metre air temperatures recorded at station Garwood Glacier (GAFM) and the values from the closest grid node of the ERA5 and BCR datasets. Time series of the AWS data (grey curve) compared to the reanalyses data (black curve) and the altitude-corrected (ac) reanalyses data (dashed orange curve) for the ERA5 (a) and BCR (b) datasets. The correlograms showing the best fit line to the relationship between the AWS temperatures and the ERA5 and BCR temperatures are shown in (c) and (d), respectively. Note the seasonal variation in the relationship, particularly the large bias during the summer months.

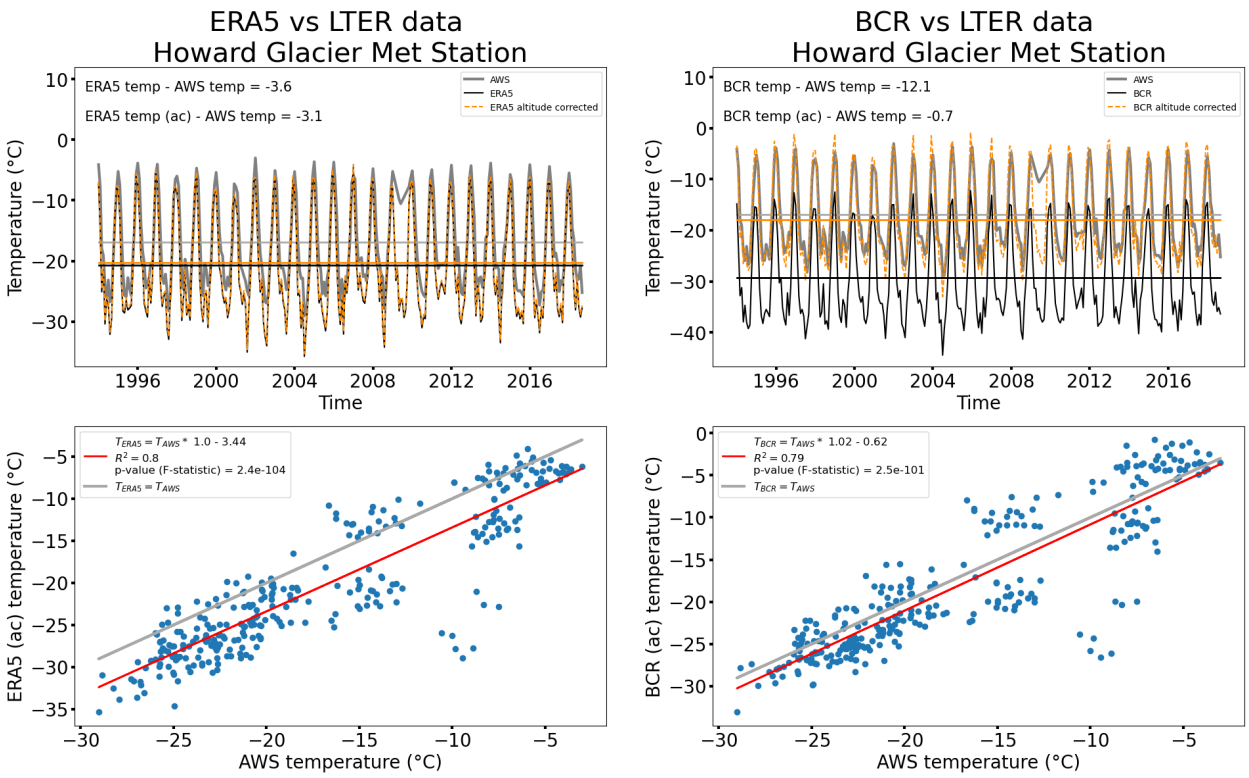

Figure S15. Comparison of the monthly averaged 2-metre air temperatures recorded at station Howard Glacier (HODM) and the values from the closest grid node of the ERA5 and BCR datasets. Time series of the AWS data (grey curve) compared to the reanalyses data (black curve) and the altitude-corrected (ac) reanalyses data (dashed orange curve) for the ERA5 (a) and BCR (b) datasets. The correlograms showing the best fit line to the relationship between the AWS temperatures and the ERA5 and BCR temperatures are shown in (c) and (d), respectively. Note the seasonal variation in the relationship, particularly the large bias during the summer months.

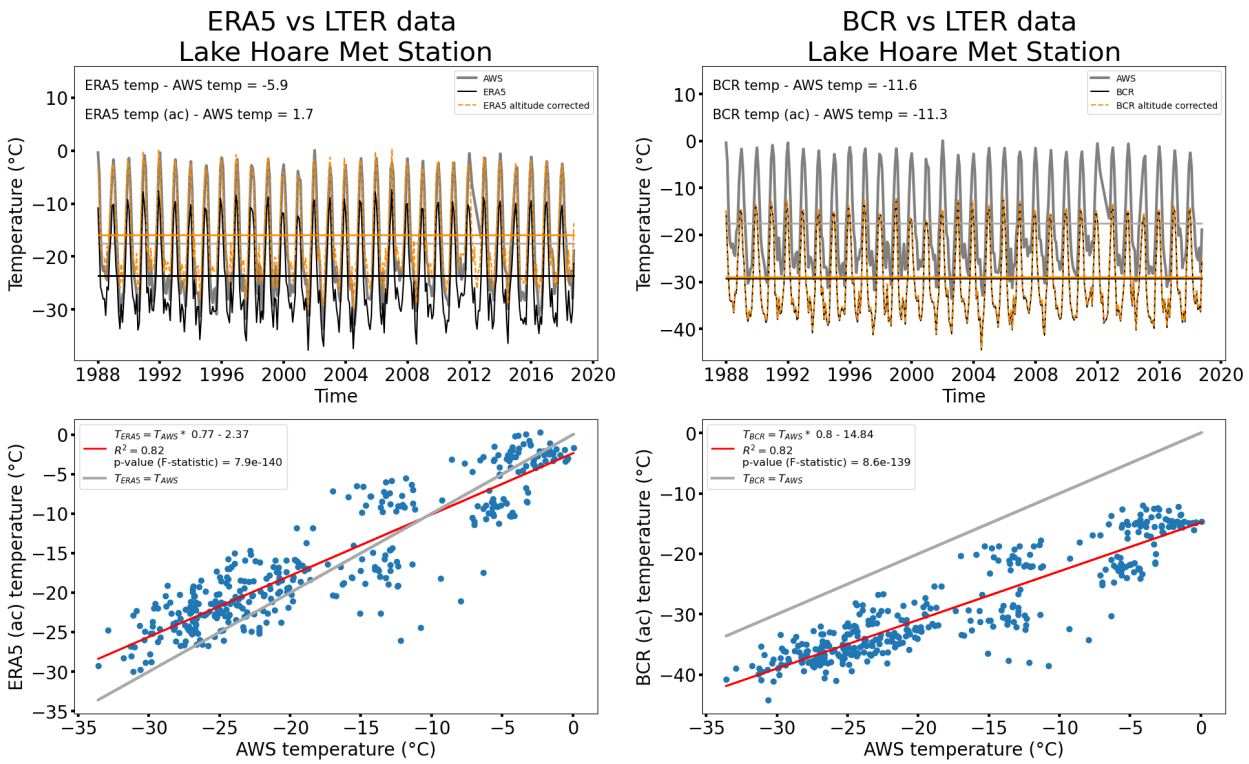

Figure S16. Comparison of the monthly averaged 2-metre air temperatures recorded at station Lake Hoare (HOEM) and the values from the closest grid node of the ERA5 and BCR datasets. Time series of the AWS data (grey curve) compared to the reanalyses data (black curve) and the altitude-corrected (ac) reanalyses data (dashed orange curve) for the ERA5 (a) and BCR (b) datasets. The correlograms showing the best fit line to the relationship between the AWS temperatures and the ERA5 and BCR temperatures are shown in (c) and (d), respectively. Note the seasonal variation in the relationship, particularly the large bias during the summer months.

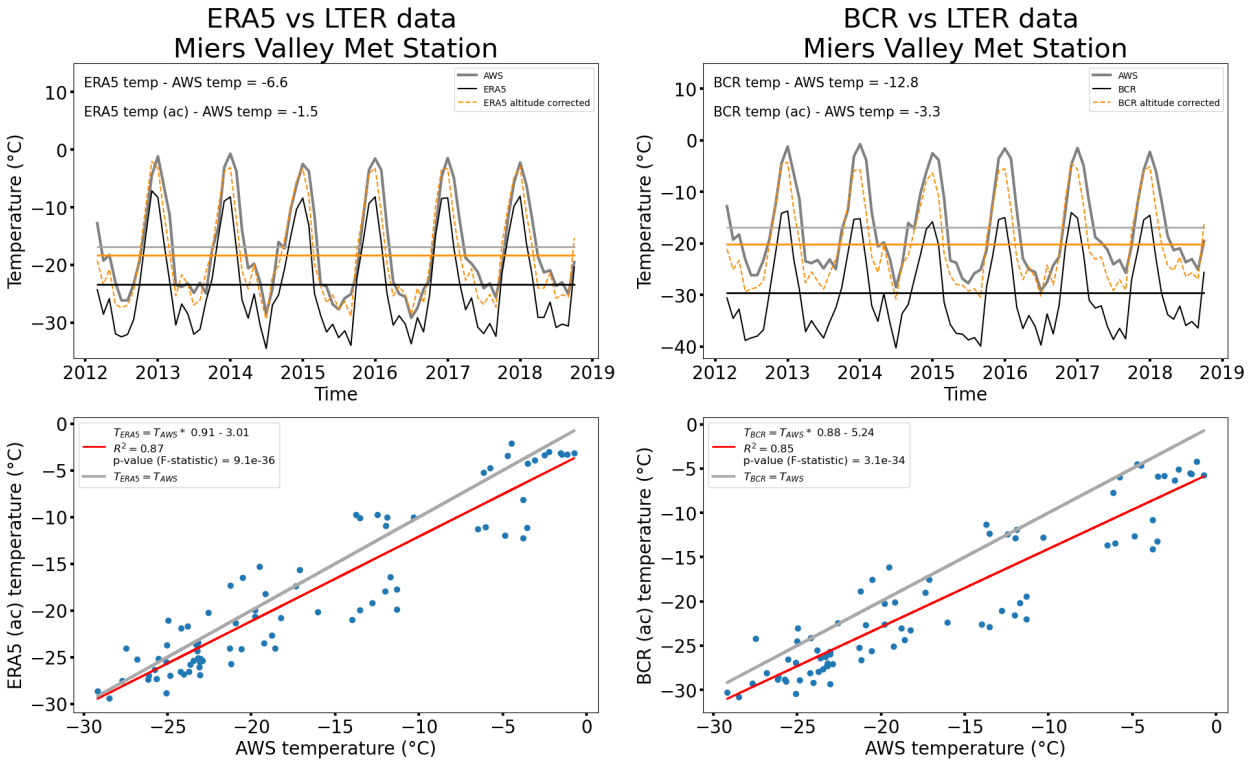

Figure S17. Comparison of the monthly averaged 2-metre air temperatures recorded at station Miers Valley (MISM) and the values from the closest grid node of the ERA5 and BCR datasets. Time series of the AWS data (grey curve) compared to the reanalyses data (black curve) and the altitude-corrected (ac) reanalyses data (dashed orange curve) for the ERA5 (a) and BCR (b) datasets. The correlograms showing the best fit line to the relationship between the AWS temperatures and the ERA5 and BCR temperatures are shown in (c) and (d), respectively. Note the seasonal variation in the relationship, particularly the large bias during the summer months.

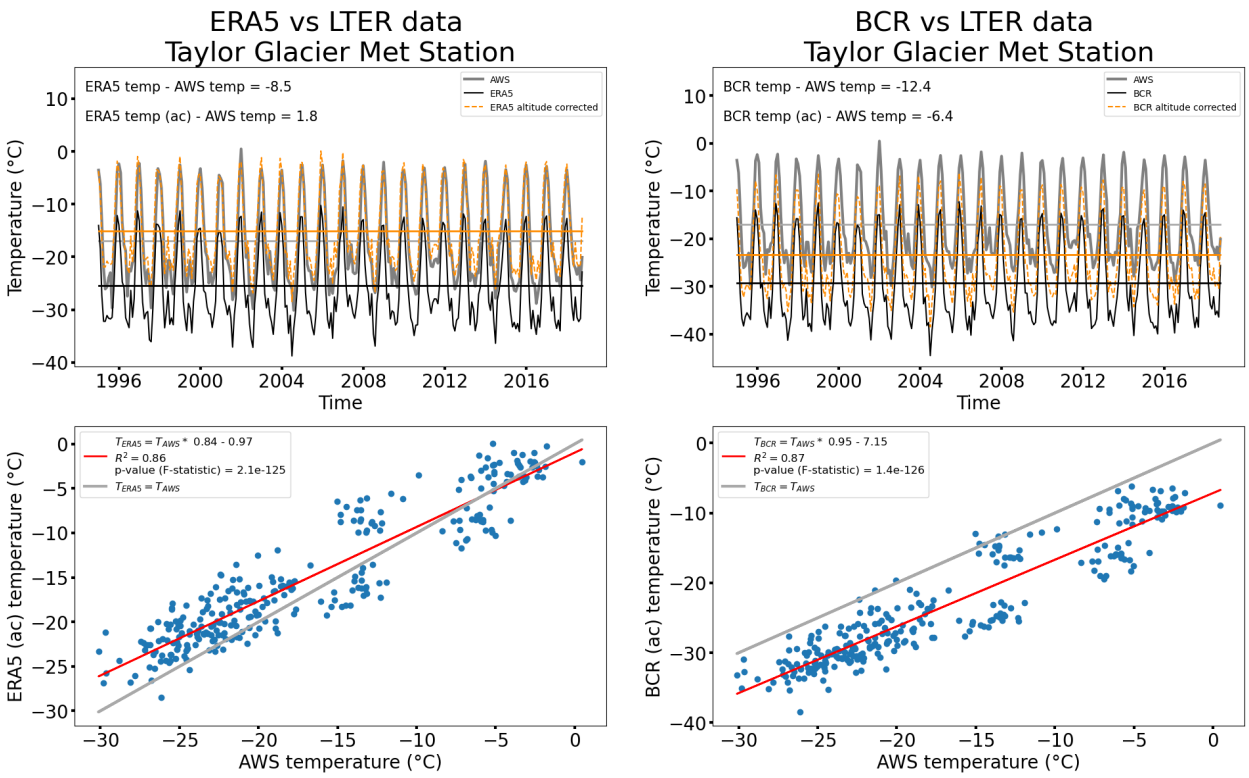

Figure S18. Comparison of the monthly averaged 2-metre air temperatures recorded at station Taylor Valley (TARM) and the values from the closest grid node of the ERA5 and BCR datasets. Time series of the AWS data (grey curve) compared to the reanalyses data (black curve) and the altitude-corrected (ac) reanalyses data (dashed orange curve) for the ERA5 (a) and BCR (b) datasets. The correlograms showing the best fit line to the relationship between the AWS temperatures and the ERA5 and BCR temperatures are shown in (c) and (d), respectively. Note the seasonal variation in the relationship, particularly the large bias during the summer months.

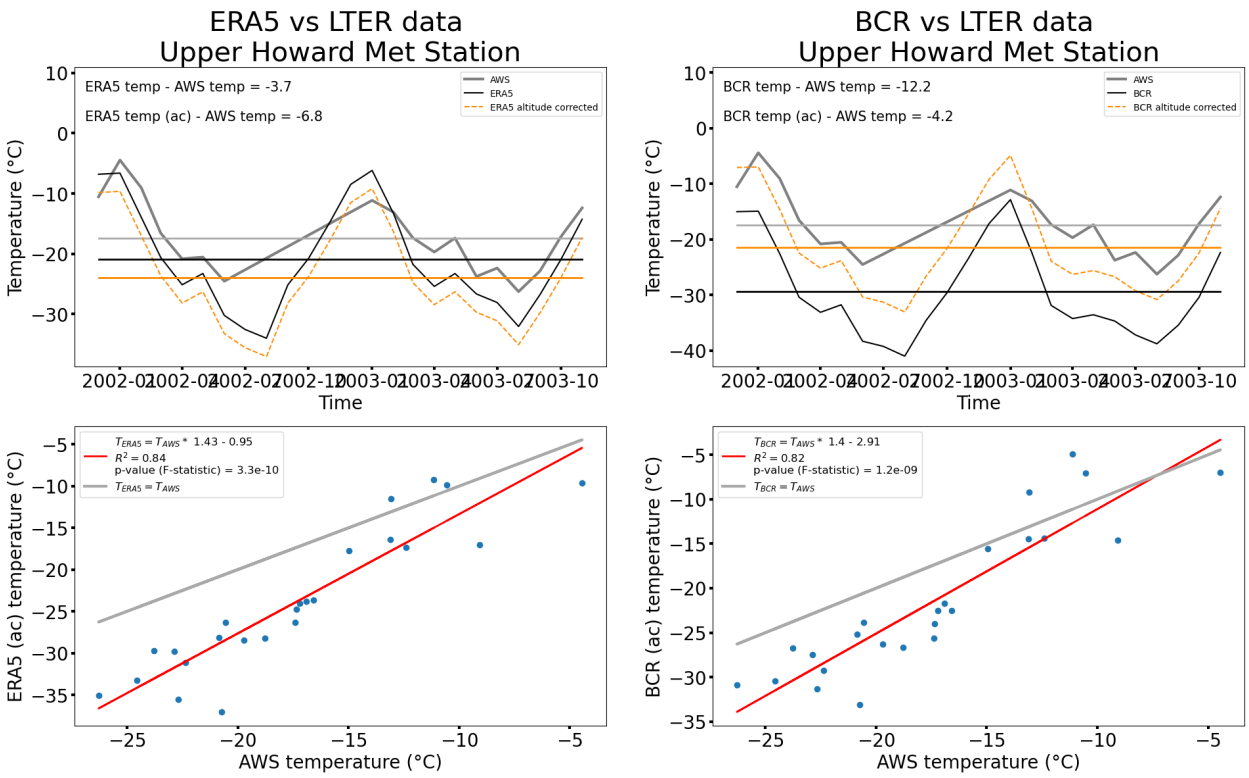

Figure S19. Comparison of the monthly averaged 2-metre air temperatures recorded at station Upper Howard (UHDM) and the values from the closest grid node of the ERA5 and BCR datasets. Time series of the AWS data (grey curve) compared to the reanalyses data (black curve) and the altitude-corrected (ac) reanalyses data (dashed orange curve) for the ERA5 (a) and BCR (b) datasets. The correlograms showing the best fit line to the relationship between the AWS temperatures and the ERA5 and BCR temperatures are shown in (c) and (d), respectively. Note the seasonal variation in the relationship, particularly the large bias during the summer months.

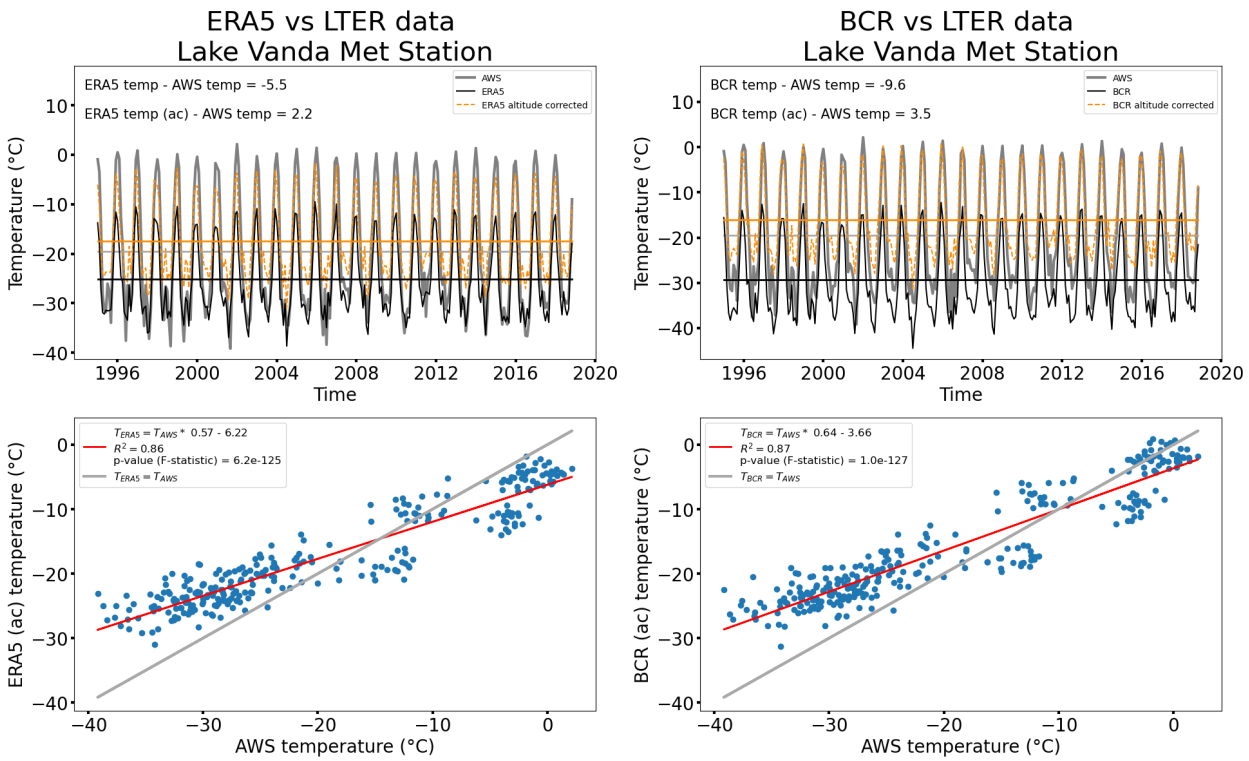

Figure S20. Comparison of the monthly averaged 2-metre air temperatures recorded at station Lake Vanda (VAAM) and the values from the closest grid node of the ERA5 and BCR datasets. Time series of the AWS data (grey curve) compared to the reanalyses data (black curve) and the altitude-corrected (ac) reanalyses data (dashed orange curve) for the ERA5 (a) and BCR (b) datasets. The correlograms showing the best fit line to the relationship between the AWS temperatures and the ERA5 and BCR temperatures are shown in (c) and (d), respectively. Note the seasonal variation in the relationship, particularly the large bias during the summer months.

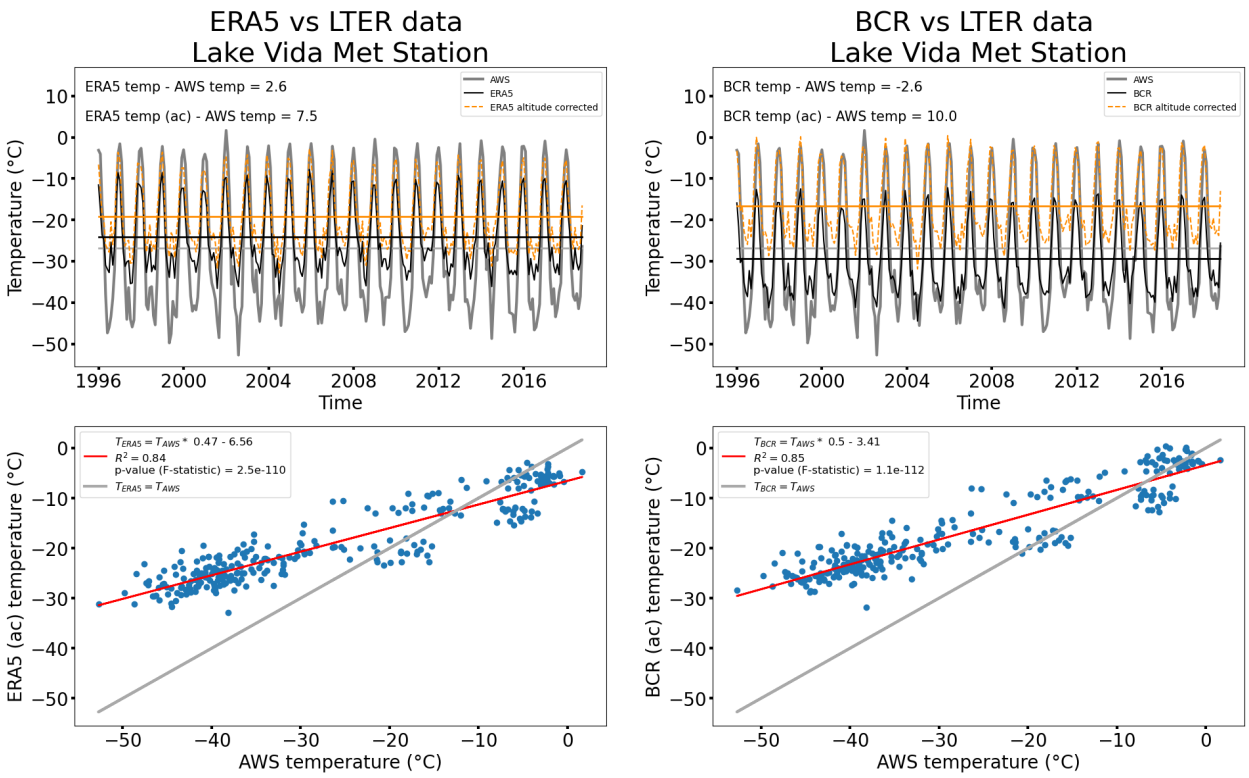

Figure S21. Comparison of the monthly averaged 2-metre air temperatures recorded at station Lake Vida (VIAM) and the values from the closest grid node of the ERA5 and BCR datasets. Time series of the AWS data (grey curve) compared to the reanalyses data (black curve) and the altitude-corrected (ac) reanalyses data (dashed orange curve) for the ERA5 (a) and BCR (b) datasets. The correlograms showing the best fit line to the relationship between the AWS temperatures and the ERA5 and BCR temperatures are shown in (c) and (d), respectively. Note the seasonal variation in the relationship, particularly the large bias during the summer months.